Typeset with jjap2.cls <ver.1.1> **Regular Paper**

Wavelength-Selectivity of Organic Photoconductive Devices by Solution Process

Takeshi FUKUDA*, Mitsuo KOMORIYA, Ryohei KOBAYASHI, Yoshihiro ISHIMARU and Norihiko KAMATA

Graduate School of Science and Engineering, Saitama University, 255 Shimo-Ohkubo, Sakura-ku, Saitama-shi, Saitama 338-8570, Japan

Organic photoconductive devices sensitive to blue, green, and red lights were achieved using poly[9,9-dioctylfluorenyl-2,7-diyl]-co-1,4-benzo-(2,1,3)-thiadiazole [F8BT], rhodamine6G-doped poly(9,9-dioctylfluorene) [PFO], nickel tetrakisi-(*tert*-butyl)phthalocyanine-doped PFO, respectively. These organic materials can be coated by a solution process, which leads us to realize the low fabrication cost and the large device area. Selectivity of spectral responses of these organic films were good enough to divide the incident light into three color components (blue, green, and red), indicating the possibility of a color separation without a prism for high resolution cameras. Quantum efficiencies of devices were estimated by absorption coefficients of photoconductive materials and photo-induced current densities while irradiating a visible light. The quantum efficiency of a blue sensitive device was better than those of green and red sensitive devices due to the suitable energy level of the blue sensitive material, F8BT.

KEYWORDS: photoconductive device, wet process, color separation, organic material, photocurrent spectra, quantum efficiency, energy diagram

1. Introduction

Recently, there have been considerable interests in organic devices due to the possibility of solution processes for further printable electronics.[1–5] Especially, organic photoconductive devices have attracted much attention from viewpoints of the lightweight and the thinness compared to other conventional image sensors, complementary metal-oxide-semiconductor sensors and charge-coupled devices. The first report of photoconductivity in organic polymers was that of H. Hoegl in poly-*N*-vinyl carbazole.[6] A photocurrent multiplication phenomenon of 10^5-fold has been observed in vacuum-evaporated films of organic semiconductors of both n-type, such as naphthalene derivative[7] and p-type, such as quinacridone.[8] In addition, an efficient high-speed organic photoconductive device has been demonstrated using a multilayer structure composed of donor-acceptor alternating layer.[9]

Most of organic materials, particularly polymers, can only be prepared by using solution processes, such as a dip-coating,[10] a spray deposition[11] and a conventional spin-coating. One

*E-mail address: fukuda@fms.saitama-u.ac.jp

serious problem of the solution process is the solvent and dust residues remained into an organic layer. Although these organic materials are coated in a nitrogen or inert atmosphere, some dust and solvent residues are still left in the organic thin films. These residues in the organic thin films cause the decrease in optical and electrical characteristics of organic devices.[12,13] In addition, the organic solution dissolves a lower organic layer during a coating process. Though a multilayer structure is efficient method to realize highly carrier injection and high quantum efficiency of organic devices,[14] some few organic materials can be used to fabricate multilayer structures by a solution process.

In the previous paper, S. Aihara et al.proposed a novel type of an image sensor overlaid with three organic photoconductive films that are individually sensitive to only one of the primary color components, blue (B), green (G), and red (R) lights,[15] respectively. In general, these organic photoconductive devices are fabricated by a conventional thermal evaporation process, and they have good reliabilities and high device performances.[16] In order to realize larger photoconductive area productivity with a lower cost, however, we need to develop solution-processed photoconductive devices at the same time. By now, very little is known about color-separable organic photoconductive devices fabricated by a solution process in our knowledge.

The purpose of this study is to investigate B, G, and R light sensitive organic photoconductive devices based on a solution process. We spin-coated photoconductive films sensitive to B, G, and R light composed of a single layer structure with poly[9,9-dioctylfluorenyl-2,7-diyl]-co-1,4-benzo-(2,1,3)-thiadiazole [F8BT], rhodamine6G [R6G]-doped poly(dioctylfluorene) [PFO], and nickel tetrakisi-(*tert*-butyl)phthalocyanine [Ni(*t*-Bu)$_4$Pc]-doped PFO, respectively. The photocurrent spectra indicate that the each photoconductive film showed good color selectivities at B, G, and R wavelength regions. In addition, we examined the external quantum efficiency (EQE), which was estimated from the absorption coefficient of an organic photoconductive neat film and the photo-induced current density while irradiating B, G, and R light, respectively.

2. Experimental

Figure 1 (a) shows a cross sectional view of fabricated organic photoconductive devices. When an incident light reaches an organic photoconductive layer through a glass substrate and an indium tin oxide (ITO) anode, it is absorbed by the organic film, resulting in generating carriers. The photo-induced carriers are accelerated by an applied electric field and finally they are read out from ITO and Al electrodes as a photocurrent. In addition, molecular structures of used organic materials, F8BT, R6G, Ni(*t*-Bu)$_4$Pc, and PFO, are shown in Fig 1 (b)

The fabrication process of these devices as follows. At first, a glass substrate covered with a patterned ITO anode was cleaned with organic solvents and deionized water under ultra sonic waves. We used F8BT for the device A, 50mol% R6G-doped PFO for the device

B, and 108mol% Ni(*t*-Bu)$_4$Pc-doped PFO for the device C as B, G, and R light sensitive photoconductive molecules, respectively. These organic materials were dissolved in chloroform as the content of 15 g/l for F8BT and R6G-doped PFO, and 10g/l for Ni(*t*-Bu)$_4$Pc-doped PFO. Following the cleaning of glass substrates, three-types of organic photoconductive materials were spin-coated on the glass substrates at a rotation speed of 1000 rpm for 60 second. Measured thicknesses were 160 nm for F8BT, 270 nm for R6G-doped PFO, and 210 nm for Ni(*t*-Bu)$_4$Pc-doped PFO as summarized in Table I, respectively. Then, chloroform was removed by baking the samples in a nitrogen atmosphere at 100 degree for 10 min. Finally, LiF and Al were thermally evaporated successively to realize efficient carrier transport between a metal cathode and an adjacent organic photoconductive layer.[17,18] Thicknesses of all the layers are shown in Table I.

Photocurrent spectra of devices were estimated by measuring the wavelength dependence of photocurrent density while irradiating the monochromic light by the fluorescence spectrometer (FP-777, JASCO). To estimate the absorption coefficient of organic photoconductive materials, ultraviolet-visible (UV-Vis) light absorption spectra of organic neat films fabricated on silica glass substrates were recorded with a UV-Vis spectrophotometer (V-550, JASCO). Monochromic light was irradiated through a glass substrate, and the transport light intensity was measured. Then, the absorption coefficient was calculated from the incident light intensity, the transport light intensity, and the thickness of an organic layer, which was measured by the surface profile meter (Dektak3, ULVAC). The positive bias voltage was applied to an ITO anode and a metal cathode.

The quantum efficiency, defined as the number of output electrons divided by the total number of irradiated photons, was estimated from the measured photocurrent and the optical intensity of irradiated light as follows.

$$\eta = \frac{I_p}{e} / \frac{P}{h\nu} \tag{1}$$

I_p, e, P, h, and ν are the measured photocurrent, the elemental charge, the irradiated optical intensity, Planck's constant, and the frequency of vibration of irradiated light, respectively. In addition, the irradiated optical intensity was calculated as the incident light intensity divided by the absorbance of the ITO layer. We used three light emitting diodes (LEDs) with center wavelengths of 469, 530, and 619 nm. The LED light was irradiated through a glass substrate and a ITO anode, and then the photocurrent was measured.

3. Results and Discussion

Figure 2 shows photocurrent spectra of the devices fabricated with photoconductive layers of F8BT for device A, R6G-doped PFO for device B, and Ni(*t*-Bu)$_4$Pc-doped PFO for device C. The wavelength of the irradiated monochromic light ranged from 400 to 800 nm. Positive

bias voltages of 1.6×10^5, 1.9×10^5, and 1.0×10^5 V/cm were applied to devices A, B, and C, respectively, during the measurement.

In the case of device A, there was a peak in the photocurrent spectrum at 465 nm; however it remained low in both cases of wavelength regions below 400 nm and above 500 nm. This result indicates that device A had sensitivity in only the B wavelength region with little response in the G and R wavelength regions. On the other hand, the center wavelength of the photocurrent spectrum of device B was 554 nm, and the photocurrent was decreased in both shorter and longer wavelengths. As a result, the incident light of the G wavelength region is only detected by the device B without sensitivities at B and R wavelengths. Furthermore, the photocurrent spectrum of device C had a peak wavelength at 610 nm with a full width at half maximum (FWHM) of about 70 nm, showing a sensitivity in only the R wavelength region, as shown in Fig. 2. In addition, absorption spectra of PFO are shown as dashed lines in Figs. 2(b) and 2(c). PFO has little absorption in the visible wavelength region. Therefore, photocurrent peaks of devices B and C correspond to absorption peaks of R6G and Ni(*t*-Bu)$_4$Pc, respectively.

These photocurrent spectra of three organic photoconductive devices clearly indicate that we can obtain color-separable organic photoconductive devices sensitive to B, G, and R wavelength regions using F8BT, R6G-doped PFO, and Ni(*t*-Bu)$_4$Pc-doped PFO as photoconductive layers, respectively. In addition, the photocurrent was rapidly increased in the shorter wavelength region below 450 nm in the case of devices B and C, because the host material (PFO) absorbs violet light, which corresponds to the energy gap of PFO between the highest occupied molecular orbital (HOMO) and lowest unoccupied molecular orbital (LUMO).[19)]

Absorption spectra of organic neat films are also shown in Fig. 2. The absorption peaks of F8BT, R6G-doped PFO, and Ni(*t*-Bu)$_4$Pc-doped PFO were 448 nm (FWHM: 85 nm), 560 nm (FWHM: 94 nm), and 609 nm (FWHM: 68 nm), respectively. These spectral shapes were similar to the photocurrent spectra of all the devices, as shown in Fig. 2. In the case of R6G-doped PFO, two peaks appeared in the G wavelength region. The absorption spectrum of R6G was similar to that of R6G-doped PFO. Therefore, these two peaks are attributed to the absorption of R6G. It is evident from Fig. 2 that irradiated light is converted into photocurrent in an organic photoconductive layer.

An organic layer over 1 μm in thickness is difficult to coat by a conventional solution process because of the low viscosity of the organic solution. Therefore, a high-absorption coefficient is necessary to realize high quantum efficiency of organic photoconductive devices by a solution process. The measured absorption coefficient of 138000 cm^{-1} at the peak position for the F8BT neat film corresponds to an absorption of 80.2 % through a thickness of 160 nm in an organic photoconductive layer of devices A, F8BT. In addition, R6G-doped PFO and Ni(*t*-Bu)$_4$Pc-doped PFO layers absorbed 97.8 % and 98.4 % of the incident light in the organic

layer of devices B (270 nm) and C (210 nm) owing to the maximum absorption coefficients of 84000 and 77000, respectively. Absorption ratios of organic layers were estimated using the equation.

$$\frac{I}{I_0} = e^{-\alpha z}. \tag{2}$$

I and I_0 are the incident and transmitted light intensities. In addition, α and z are the absorption coefficient and the thickness of the organic layer, respectively. Although the photoconductive layer is thin, approximately 200 nm for all the devices, the absorption coefficient is sufficiently high to absorb the incident light, resulting in the generation of efficient carriers by the light irradiation.

Figure 3 represents the external quantum efficiency (EQE) defined as the number of photoinduced carriers divided by the number of irradiated photons. The EQE was estimated from the absorption coefficient of an organic neat film and the measured current density-voltage characteristics while irradiating visible light on an organic photoconductive layer through a glass substrate. The center wavelengths of irradiated light-emitting diodes were 469, 530, and 619 nm for devices A, B, and C, respectively. The pulse duration was 50 ms to avoid thermal damage to the organic layer by light irradiation. The irradiated optical intensity was about 1 mW/cm^2, and the EQE had no effect on the irradiated optical intensity below 10 mW/cm^2. In addition, a bias voltage was also applied to the device during the measurement of the photoinduced current density. The electric field was calculated as the applied voltage divided into the thickness of the organic layer, 160 nm for F8BT, 270 nm for R6G-doped PFO, and 210 nm for Ni(*t*-Bu)$_4$Pc-doped PFO. The electric field ranged from 0.2×10^5 to 2.2×10^5 V/cm.

As shown in Fig. 3, the EQEs of all the devices increased constantly with increasing electric field. The trend is due to the acceleration of photoinduced carriers by an electric field.[15] The carrier diffusion length for most organic materials is below 20 nm,[20] which is less than the thickness of an organic photoconductive layer. In addition, the carrier mobility of organic materials is increased as the applied electric field increases.[21] Therefore, a higher electric field causes the dissociated hole-electron pairs in an organic photoconductive material with low recombination probability, resulting in higher EQE, as shown in Fig. 3.

The experimental result shown in Fig. 3 indicates that the maximum EQE of device A was 0.12% at an applied electric field of 2.2×10^5 V/cm, implying approximately 10 and 100 times higher values than those of devices B and C. The EQEs of devices B and C were 0.009% at 1.5×10^5 V/cm and 0.001% at 1.7×10^5 V/cm, respectively. The higher EQE of device A can be explained by the energy diagrams of organic photoconductive devices. Figure 4 shows the energy diagrams of three devices. Here, HOMO and LUMO levels were estimated from PL and absorption spectra of organic neat films. The work function of LiF/Al is 3.1 eV.[22]

Since the HOMO levels of F8BT and PFO are 5.9 and 5.8 eV, respectively,[19,23,24] the

hole-injection efficiencies at an ITO-organic interface are considered to be almost the same for all the devices. On the other hand, the LUMO level of F8BT was 3.3 eV,[19] which was higher than that of PFO, 2.6 eV.[23,24] The energy gap differences at LUMO/HOMO levels of organic photoconductive layers were 0.6/0.3 and 0.0/0.8 eV for devices B and C, respectively. The large energy gap prevents carrier transfer between donor-acceptor materials, and PFO acts as a potential barrier of photoinduced electron-hole pairs rather than as a carrier transport material, resulting in the highest EQE of device A. In addition, the hole mobility of F8BT is higher than the electron mobility of F8BT.[19] Therefore, the smaller energy gap of the LUMO level at an organic-metal interface is considered to cause efficient carrier dislocation in the F8BT layer.

LUMO levels of Ni(*t*-Bu)$_4$Pc and PFO were approximately the same, and hence photoinduced electrons are easily recombined with photoinduced holes of the HOMO level, because the energy gap at the PFO-LiF/Al interface is large, approximately 0.5 eV, resulting in the generation of an electron trap in PFO. On the other hand, differences in LUMO and HOMO levels of R6G and PFO were 0.6 and 0.3 eV, respectively. In the case of device B, photoinduced carriers are transported in energy levels of PFO with lower carrier recombination probability than device C. Therefore, the EQE of device C is lower than that of device B.

4. Conclusions

We demonstrated color-selectable organic photoconductive devices fabricated by a spin-coating process. The photocurrent spectra of all the devices showed good spectral selectivity at B, G, and R wavelength regions using F8BT, R6G-doped PFO, and Ni(*t*-Bu)$_4$Pc-doped PFO as photoconductive layers, respectively. EQEs of all the devices were estimated using the measured absorption coefficient and the photocurrent, and we found that alignment of energy levels of organic layers is important to increase device performance. In addition, these results indicate that printable organic photoconductive devices can be fabricated on a plastic substrate using a solution process, and high-resolution, high-efficiency, and light weight image sensors are predicted for practical use in the near future. To obtain a color image, a solid-state circuit that reads out signals generated in the organic photoconductive layer will be necessary. Combining readout circuits with these devices could lead to the realization of practical organic image sensors.

Acknowledgment

This work was supported by "Development of functional optical materials and devices for next generation in frontier photonics", Regional New Consortium of the Ministry of Economy, Trade and Industry.

References

1) S. Nakano, T. Sekitani, T. Yokota, and T. Someya: Appl. Phys. Lett. **92** (2008) 053302.
2) J. A. Hauch, P. Schilinsky, S. A. Choulis, R. Childers, M. Biele, and C. J. Brabec: Sol. Energy Mater. Sol. Cells **92** (2008) 727.
3) D. Wang, X. Gong, P. S. Heeger, F. Rininsland, G. C. Bazan, and A. J. Heeger: Proc. NaH. Acad. Sci. U. S. A.**99** (2002) 49.
4) T. Fukuda, B. Wei, M. Ichikawa, and Y. Taniguchi: Jpn. J. Appl. Phys. **46** (2007) 7880.
5) N. Kamata, D. Terunuma, R. Ishii, H. Satoh, S. Aihara, Y. Yaoita, and S. Tonsyo: J. Organomet. Chem. **685** (2003) 235.
6) H. Hoegl: J. Phys. Chem. **69** (1965) 755.
7) T. Katsume, M. Hiramoto, and M. Yokoyama: Appl. Phys. Lett. **69** (1996) 3722.
8) M. Hiramoto, S. Kawase, and M. Yokoyama: Jpn. J. Appl. Phys. **35** (1996) L349.
9) P. Peumans, V. Bulovic, and S. R. Forrest: Appl. Phys. Lett. **76** (2000) 3855.
10) P. Yimsiri and M. R. Mackley: Chem. Eng. Sci. **61** (2005) 3496.
11) M. Shakutui, K. Fujita, and T. Tsutsui: Jpn. J. Appl. Phys. **45** (2006) L790.
12) B. Geffroy, P. le Roy, and C. Prat: Polym. Int. **55** (2006) 572.
13) D. A. Pardo, N. Peyghambarian, and G. E. Jabbour: Jpn. J. Appl. Phys. **40** (2001) 4922.
14) C. W. Tang and S. A. V. Slyke: Appl. Phys. Lett. **51** (1987) 913.
15) S. Aihara, Y. Hirano, T. Tajima, K. Tanioka, M. Abe, N. Saito, N. Kamata, and D. Terunuma: Appl. Phys. Lett. **82** (2003) 511.
16) H. Seo, S. Aihara, T. Watabe, H. Ohtake, M. Kubota, and N. Egami: Jpn. J. Appl. Phys. **46** (2007) L1240.
17) L. S. Hung, C. W. Tang, and M. G. Mason: Appl. Phys. Lett. **70** (1997) 152.
18) J. Kido and T. Matsumoto: Appl. Phys. Lett. **73** (1998) 2866.
19) L. -L. Chua, J. Zaumseil1, J.-F. Chang, E. C.-W. Ou, P. K.-H. Ho, H. Sirringhaus, and R. H. Friend: Nature **434** (2005) 194.
20) H. Hoppe, and N. S. Sariciftci: J. Mater. Res. **19** (2004) 1924.
21) S. Barth, P. Müller, H. Riel, P. F. Seidler, W. Rieβ, H. Vestweber, and H. Bässler: J. Appl. Phys. **89** (2001) 3711.
22) D. H. Chung, S. W. Hur, S. K. Kim, J. U. Lee, C. H. Kim, J. W. Hong, and T. W. Kim: Curr. Appl. Phys. **4** (2004) 667.
23) X. Gong, D. Moses, A. J. Heeger and S. Xiao: Synth. Met. **141** (2004) 17.
24) J. Hwang and A. Kahna: J. Appl. Phys. **97** (2005) 103705.

Figure captions

Figure 1. (a) Cross sectional view of three organic photoconductive devices with F8BT (device A), R6G-doped PFO (device B), and Ni(*t*-Bu)$_4$Pc-doped PFO (device C) as photoconductive layers. (b) Molecular structures of organic materials in this study.

Figure 2. Solid lines shows spectral photoresponse characteristics of three devices with F8BT (device A), R6G-doped PFO (device B), and Ni(*t*-Bu)$_4$Pc-doped PFO (device C) as photoconductive layers, respectively. Dotted lines shows UV-vis absorption spectra of F8BT, R6G-doped PFO, and Ni(*t*-Bu)$_4$Pc-doped PFO neat films. Dashed curve in (b) and (c) is absorption spectra of PFO.

Figure 3. EQEs of three organic photoconductive devices as a function of an applied electric field. Devices A, B, and C were excited by visible LEDs with center wavelengths of 469, 530, and 619 nm, respectively.

Figure 4. Energy diagrams of devices A, B, and C with (a) F8BT, (b) R6G-doped PFO, and (c) Ni(*t*-Bu)$_4$Pc-doped PFO as photoconductive layers, respectively.

Table I. Device structures sensitive to B (device A), G (device B), and R (device C) wavelength regions.

Color	Device structure
Blue (device A)	ITO (150 nm)/F8BT (160 nm)/LiF (0.5 nm)/Al (150 nm)
Green (device B)	ITO (150 nm)/R6G:PFO (270 nm)/LiF (1.0 nm)/Al (150 nm)
Red (device C)	ITO (150 nm)/Ni(*t*-Bu)$_4$Pc:PFO (210 nm)/LiF (1.0 nm)/Al (150 nm)

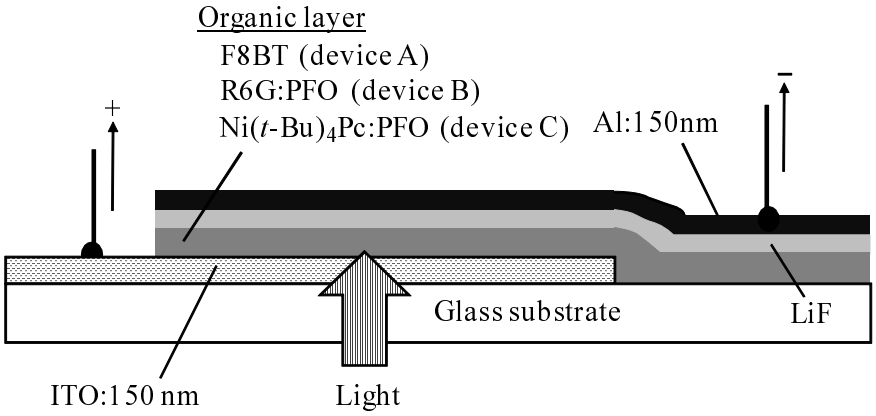

(a)

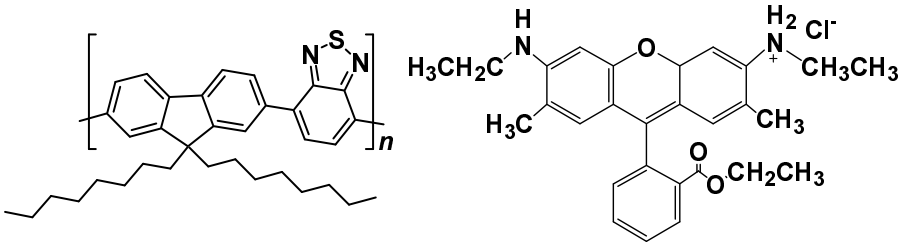

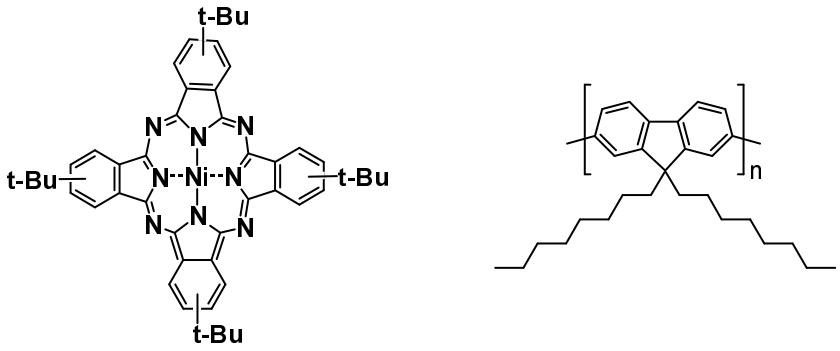

(b)

Fig. 1. (a) The cross sectional view of three-types of organic photoconductive devices with F8BT (device A), R6G-doped PFO (device B), and Ni(t-Bu)$_4$Pc-doped PFO (device C) as photoconductive layers, respectively. (b) Molecular structures of used organic materials in this study.

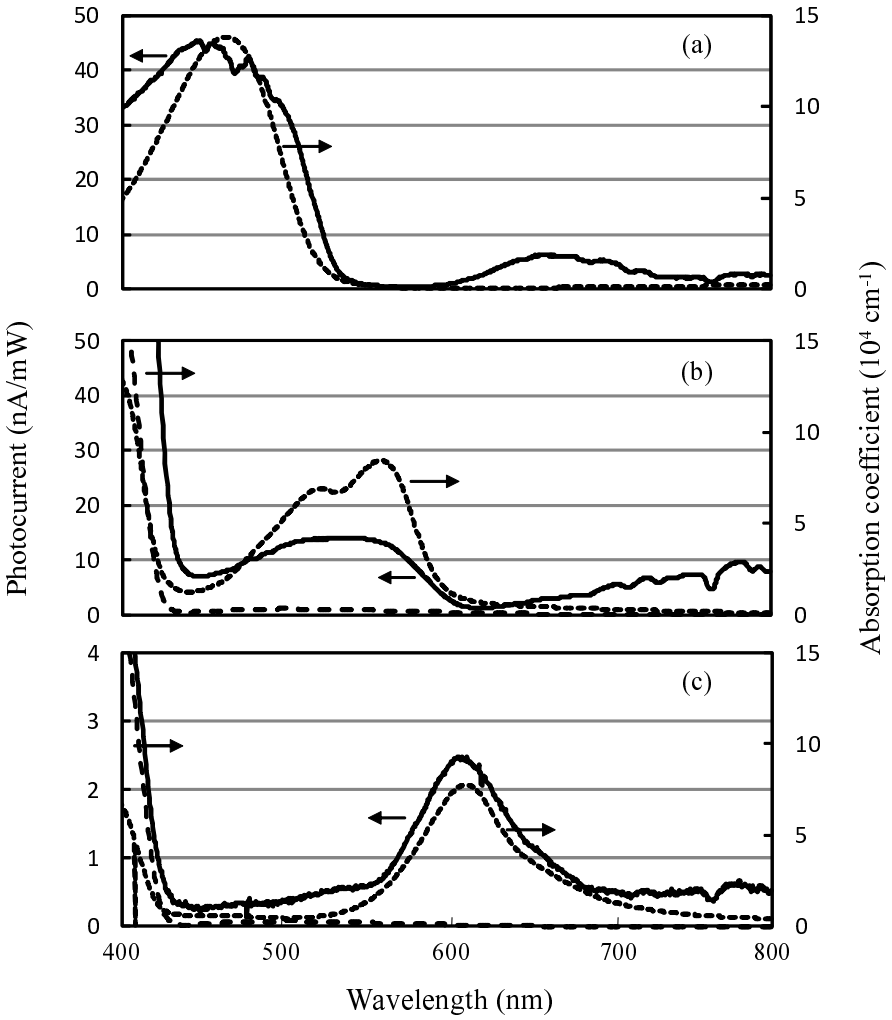

Fig. 2. Solid lines shows spectral photoresponse characteristics of three devices with F8BT (device A), R6G-doped PFO (device B), and Ni(t-Bu)$_4$Pc-doped PFO (device C) as photoconductive layers, respectively. Dotted lines shows UV-vis absorption spectra of F8BT, R6G-doped PFO, and Ni(t-Bu)$_4$Pc-doped PFO neat films. Dashed curve in (b) and (c) is absorption spectra of PFO.

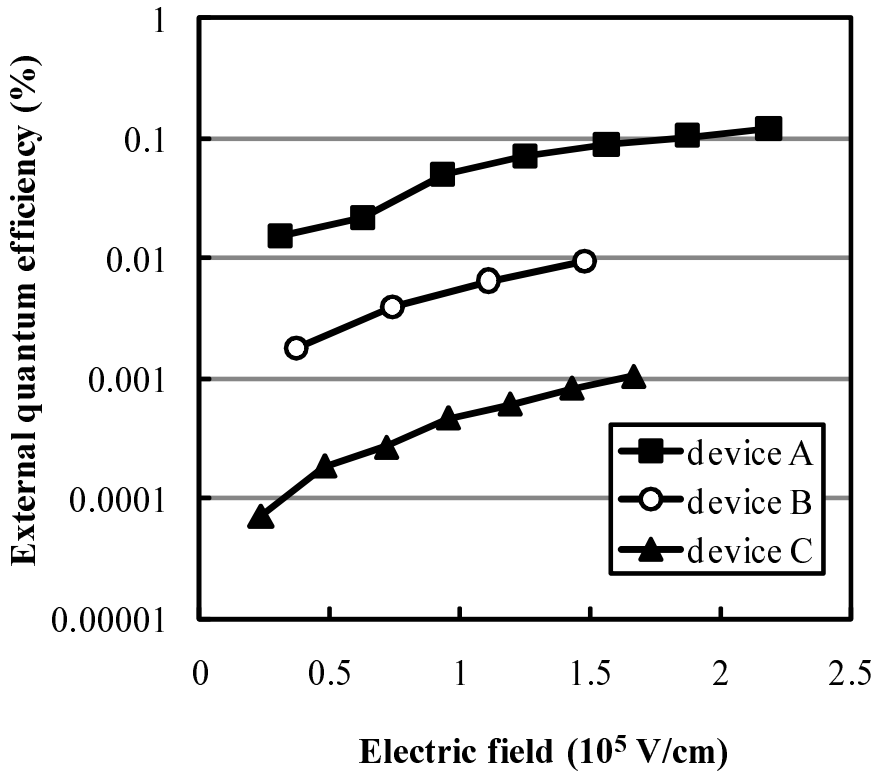

Fig. 3. EQEs of three organic photoconductive devices as a function of an applied electric field. Devices A, B, and C were excited by visible LEDs with center wavelengths of 469, 530, and 619 nm, respectively.

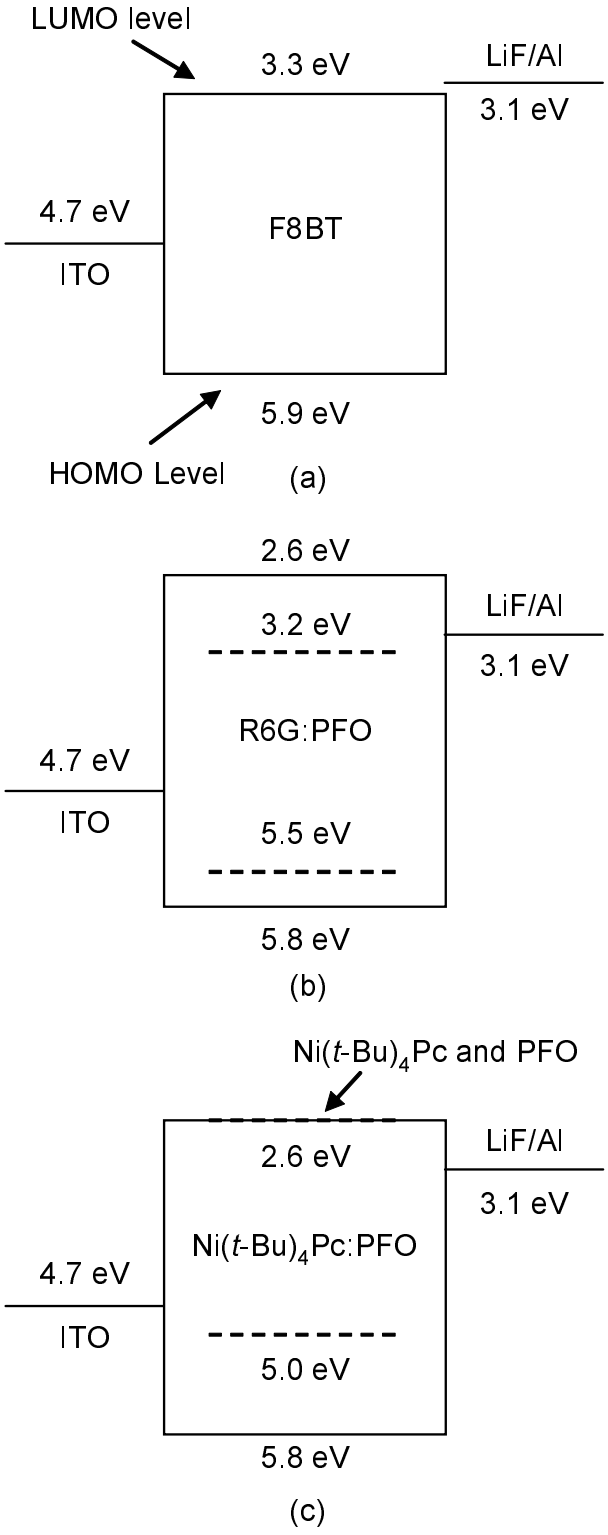

Fig. 4. Energy diagrams of devices A, B, and C with (a) F8BT, (b) R6G-doped PFO, and (c) Ni(*t*-Bu)$_4$Pc-doped PFO as photoconductive layers, respectively.